Received: 12 August 2020 | Revised: 26 October 2020 | Accepted: 4 November 2020

DOI: 10.1049/els2.12012

IET Electrical Systems in Transportation

The Institution of Engineering and Technology WILEY

ORIGINAL RESEARCH PAPER

SRM power density improvement utilising rotor conducting screens and DC-link voltage boosting for EV applications

Aly A. Abdel-Aziz[1] | **Khaled H. Ahmed**[1,2] | **Ahmed M. Massoud**[3] | **Barry W. Williams**[1]

[1]Department of Electronic and Electrical Engineering, University of Strathclyde, Glasgow, UK

[2]Department of Electrical Engineering, Faculty of Engineering, Alexandria University, Alexandria, Egypt

[3]Department of Electrical and Computer Engineering, Texas A&M University at Qatar, Doha, Qatar

Correspondence

Aly A. Abdel-Aziz, Department of Electronic and Electrical Engineering, University of Strathclyde, Glasgow, G1 1XQ, UK.
Email: aly.abdelaziz@rocketmail.com

Funding information

Qatar National Research Fund, Grant/Award Number: NPRP (9-092-2-045)

Abstract

The power density enhancement of a four-phase switched reluctance motor using rotor conducting screens and DC-link voltage boosting for electric vehicle applications is studied. The effect of conducting screen thickness and material electrical conductivity on current rise time, developed torque, and output power is studied. Different screen shapes are compared that elicit the optimum screen design by formulating a multi-objective optimisation problem based on maximising the developed torque and efficiency and minimising added material weight. A double arm common switch converter with a DC-link voltage-boosting capacitors is deployed. The boosted voltage provided by the capacitors aids the winding current to rapidly build-up; thus, increasing the motor base speed, whence power rating. Finite element analysis results confirm the SRM drive's effectiveness in increasing the motor base speed and improving the torque range; hence make the power capability of SRMs to be competitive with an equivalent volume permanent magnet synchronous motor.

1 | INTRODUCTION

The global climate change crisis has urged researchers to explore cleaner energy systems. The transportation sector is placed second in carbon emission. Transportation electrification is thus a key solution for a greener environment [1].

Several electrical machine types are available to support performing this transportation electrification task viz., the permanent magnet synchronous machine (PMSM), the squirrel cage induction machine (SCIM), and the switched reluctance machine (SRM) [2, 3]. Due to its high power density along with a desirable constant power operating region, the PMSM is considered the most suitable machine option for automobiles. Nonetheless, limited resources and escalated prices of rare-earth materials, which is indispensable for the PMSM, have forced the market to search for a rare-earth free machine [4].

Among the available alternatives, the SRM stands as a promising candidate for drivetrains [5]. Its simple and rigid construction, fault-tolerant capability, high torque, and wide constant power range are among the SRM merits. The absence of PMs and rotor windings simplifies motor geometry [6]. Despite the SRM advantages, it has a lower power density compared with the PMSM [7, 8]. Schemes have been proposed to improve power density [9, 10]. The new machine designs are competitive with the PMSM in terms of power density and efficiency [11–13].

In simplistic terms, the current into and out of an SRM (at phase current turn-on and turn-off) can be expressed by

$$V = \pm L \frac{di}{dt} \tag{1}$$

The objective is to force the current into and out of the machine as quickly as possible through maximising the di/dt term, thereby increasing the base-speed, whence output power. The inductive term L is related to the machine design, and specifically low L (for V fixed) at only phase turn-on will maximise the machine co-energy. Alternatively, di/dt (at both phase turn-on and turn-off) can be increased by increasing the term V, which is a converter parameter. Thus, both machine and converter design can independently impact the machine torque and power density.

This is an open access article under the terms of the Creative Commons Attribution License, which permits use, distribution and reproduction in any medium, provided the original work is properly cited.

© 2021 The Authors. *IET Electrical Systems in Transportation* published by John Wiley & Sons Ltd on behalf of The Institution of Engineering and Technology.

20429746, 2021, 2, Downloaded from https://ietresearch.onlinelibrary.wiley.com/doi/10.1049/els2.12012 by NHS Education for Scotland NES, Edinburgh Central Office, Wiley Online Library on [14/11/2022]. See the Terms and Conditions (https://onlinelibrary.wiley.com/terms-and-conditions) on Wiley Online Library for rules of use; OA articles are governed by the applicable Creative Commons License

From a machine design perspective, the concept of flux screens was proposed in Ref. [14] to increase the output torque. Electrical conducting, non-magnetic materials such as aluminium or copper, are inserted in the rotor's interpole regions. The conducting screens encounter a time-varying flux due to motor rotation, which induces a voltage. The induced voltage produces eddy currents, producing flux that opposes the original stator pole flux. The opposing flux results in a decrease in the effective unaligned inductance. However, the impact of reducing the unaligned inductance on the developed torque was not positive in a three-phase 6/4 SRM [14]. In Refs. [15–17], the rotor conducting screens were tested for four-phase (8/6), two-phase (4/2), and single-phase (2/2) SRM, respectively. Although the deployment of rotor conducting screens improved SRM torque per unit volume, the effect of thickness, shape, and material of the conducting screens on SRM performance was not investigated. Also, the SRM power density (increase in base-speed at full-load torque) with rotor conducting screens is less than that of an equivalent PMSM.

From a converter design perspective and increasing the base-speed hence output power, in the single-phase SRM in Refs. [18] and [19], the converter DC-link voltage has been boosted with a series-diode plus shunt-capacitor inserted after the DC source. The boosted voltage provided by the capacitor aids the winding current to rapidly build-up; thus, increasing the motor base-speed. The application of the boost-capacitor was extended to poly-phase SRM in Refs. [20–22]. Nevertheless, the current overlap between incoming and outgoing phases reduces the boosting-voltage effect. In Refs. [23] and [24], the problem of phase current overlap in a four-phase SRM was resolved using a double arm topology with two boost capacitors, one for each arm. Above the improved base-speed, the current is limited by the ever-increasing effective back EMF. Adversely, using low capacitance for a higher boost voltage implies an increased semiconductor voltage rating requirement.

Herein, the utilisation of rotor conducting screens and DC-link voltage boosting for a four-phase SRM is investigated for electric vehicle (EV) applications. The conducting screens reduce the effective unaligned inductance allowing the phase turn-on current to build-up faster, hence increasing SRM torque per unit volume, especially at high speeds. The effect of thickness and material resistivity of the conducting screens on the SRM performance is discussed. Different rotor conducting screen shapes are compared with respect to the weight of added material, developed torque, and efficiency to choose the optimum design.

Moreover, a double-arm common switch converter with voltage-boosting capability is assessed. The de-magnetisation energy of the outgoing phase is stored in the capacitors, effectively increasing the opposing voltage. This, in turn, decreases the current fall time, thereby efficiently extending the positive torque production range before operating in the negative torque region. The stored energy (which increases the DC-link voltage) then feeds the next incoming phase, thus allowing faster current build-up, which (in conjunction with the reduced current fall time at phase turn-off) increases the motor base-speed. The converter also allows regenerative energy to be fed-back to the supply instead of being dissipated for rapid machine regenerative braking. The proposed drive system improves SRM power density to be competitive with an equivalent PMSM, thus satisfying the need for EV applications.

The contribution of this work can be summarised as follows:

- Investigation of the effect of utilising rotor conducting screens with different materials, thicknesses, and shapes on SRM performance.
- Formulation of a multi-objective optimisation problem to elicit the optimum screen shape with respect to the developed torque, efficiency, and weight of added material.
- Improving the power density of SRM utilising rotor conducting screens and voltage boosting to be competitive with an equivalent sized PMSM.

Herein, Section 2 highlights the salient SRM features. Section 3 briefly summarises the converter operation with voltage-boosting capacitors. The concept of rotor conducting screens is demonstrated in Section 4. Section 5 investigates the effect of utilising rotor conducting screens with different materials, thicknesses, and shapes on the performance of SRM. Besides, a multi-objective optimisation problem is formulated to choose the best screen with respect to developed torque, efficiency, and weight of added material. Section 6 considers SRM improved performance with DC-link voltage boosting, while Section 7 considers performance with both rotor screens and DC-link voltage boosting. Section 8 represents the conclusion of the studied SRM.

2 | FUNDAMENTALS OF SRM

The SRM is a double salient machine with a concentrated winding on each stator pole, without windings or permanent magnets on the rotor [25]. Air-gap reluctance dominates the unaligned reluctance resulting in linear flux linkage-current, $\lambda-i$, characteristics. However, core reluctance cannot be neglected in the aligned position, whence the $\lambda-i$ characteristics become non-linear, as shown in Figure 1.

Torque is produced by rotor poles' tendency to align with excited stator poles, minimising the flux path's reluctance. Equation (2) defines the torque.

$$T = \frac{\partial W_f'(\theta, i)}{\partial \theta} \tag{2}$$

where θ is the rotor position. The co-energy $W_{\mathrm{f}}^{'}$ is conventionally expressed in terms of flux linkage, and if saturation is neglect, linear inductance L is obtained. Then, the torque can be simplified to:

$$T = \tfrac{1}{2} i^2 \frac{\partial L(\theta, i)}{\partial \theta} \tag{3}$$

20429746, 2021, 2, Downloaded from https://ietresearch.onlinelibrary.wiley.com/doi/10.1049/elp2.12012 by NHS Education for Scotland NES, Edinburgh Central Office, Wiley Online Library on [14/11/2022]. See the Terms and Conditions (https://onlinelibrary.wiley.com/terms-and-conditions) on Wiley Online Library for rules of use; OA articles are governed by the applicable Creative Commons License

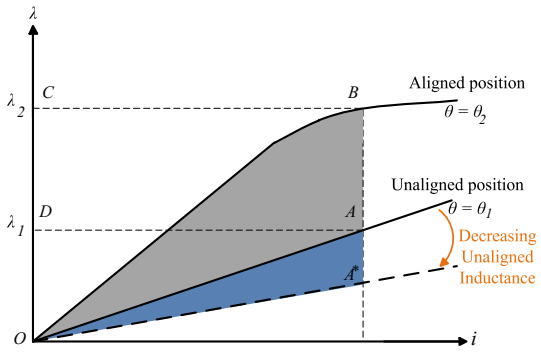

FIGURE 1 Flux linkage-current (λ-i) characteristics

Equation (3) shows that the developed torque depends on the rate of change of inductance with respect to the rotor position. The torque depends on the conversion area OAB, which is the increase in co-energy when the rotor moves from the unaligned to the aligned position. Increasing the conversion area will, in turn, increase the motor output torque.

If the mutual effect between the different phases is ignored, the voltage equation is expressed as follows:

$$V_{DC} = iR + L(\theta, i)\frac{di}{dt} + i\omega\frac{dL(\theta, i)}{d\theta} \tag{4}$$

where V_{DC} is the applied voltage, R is the phase winding resistance, and ω is the rotor speed. Using (4), the current expression at turn-on is:

$$i(t) = \frac{V_{DC}}{R_{eq}}\left(1 - e^{-t/\zeta}\right) \tag{5}$$

where R_{eq} and ζ are the equivalent resistance and time constant defined by (6) and (7), respectively.

$$R_{eq} = R + \omega\frac{dL(\theta_{on}, i)}{d\theta} \tag{6}$$

$$\zeta = \frac{L(\theta_{on}, i)}{R_{eq}} \tag{7}$$

Reducing the effective unaligned inductance (which results in a reduction in the time constant ζ) by deploying rotor conducting screens, as well as raising the DC-link voltage V_{DC} using the boost capacitors will force the current increase quickly through the motor's winding. Thus, this increases the developed torque and base-speed of the SRM and enhances its power density. At phase turn-off, only increasing the DC-link voltage (with boosting) can increase the phase current rate of decrease. Rotor conducting screen is not effective in improving performance near alignment.

3 | CONVERTER OPERATION

Figure 2 shows an asymmetric converter for a four-phase SRM [23, 24]. The converter uses the double bridge topology with quadrature phases A and C in one bridge, sharing a common leg incorporating switch S_1. The other two phases, B and D, are in an independent bridge with a common switch S_4. The DC-link blocking diodes D_{x2}, D_{y2}, and capacitors C allow boosting of the DC-link voltage by forcing recovered current to charge the capacitors to voltages in excess of the DC source V_{DC}. The increasing capacitor voltage increases the phase current fall rate at turn-off. The increase in DC-link voltage will accelerate the current build-up yielding an increase in motor base-speed. The two-independent bridge topology allows better voltage boosting (since no phase overlap occurs in each bridge) with a minimal number of switches. The DC-link switch S_{xy} (and diodes D_{x1} and D_{y1}) is for regeneration. The analysis of this converter in the motoring and braking modes is briefly highlighted in the following sub-section.

3.1 | Motoring mode

In motoring mode, the DC-link switch S_{xy} is off, and link diodes D_{x2} and D_{y2} conduct. Current is injected into the appropriate phase winding during the increasing inductance region. According to the states of the phase switches, the converter has three voltage levels, summarised in Table 1.

Figure 3 shows the typical phase voltage and current waveforms in single-pulse mode (at and above base-speed).

3.2 | Braking mode

The braking circuitry, shown in Figure 2, consists of two directing/blocking diodes (D_{x1} and D_{y1}) and a single switch, S_{xy}, which is used to bypass the boosting circuitry and is not involved in the boosting and motoring mechanisms. Thus the boosting mechanism is bypassed and not involved with braking and regeneration. Details of the braking operation of the circuit are outlined in Ref. [24].

4 | ROTOR CONDUCTING SCREENS

Torque is dependent on the difference between the aligned and unaligned inductances, and increasing this difference produces more torque and hence, output power.

To decrease the unaligned inductance (without affecting the aligned inductance), the spaces between rotor poles could be filled with non-magnetic, electrically conducting material such as aluminium or copper, as shown in Figure 4. This material is referred to as the conducting screen. The conducting screens are isolated from the rotor, and there is no electrical connection between the conducting screens.

Due to motor rotation along with stator coil excitation, the conducting screens encounter a time-varying flux, which in turn

20429746, 2021, 2, Downloaded from https://ietresearch.onlinelibrary.wiley.com/doi/10.1049/elp2.12012 by NHS Education for Scotland NES, Edinburgh Central Office, Wiley Online Library on [14/11/2022]. See the Terms and Conditions (https://onlinelibrary.wiley.com/terms-and-conditions) on Wiley Online Library for rules of use; OA articles are governed by the applicable Creative Commons License

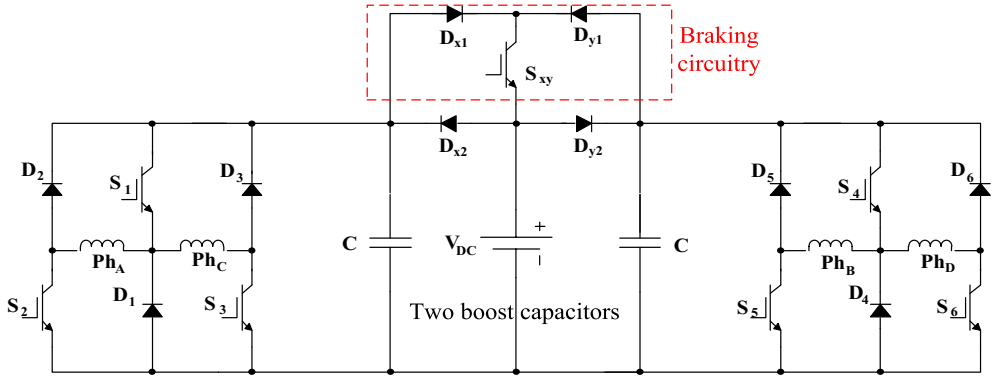

FIGURE 2 SRM 8/6 converter with DC-link capacitor voltage boosting

TABLE 1 Converter output voltage states

Level	State/ KVL	Initial voltage	Final voltage	Capacitor voltage
$+V_{DC}$	C, S_1, S_2	$+V_{DC} + V_{Boost}$	$+V_{DC}$	C ↓
$0V$	D_2, S_1	V_{DC}	V_{DC}	C ↔
	D_1, S_2			
$-V_{DC}$	D_2, C, D_1	V_{DC}	$V_{DC} + V_{Boost}$	C ↑

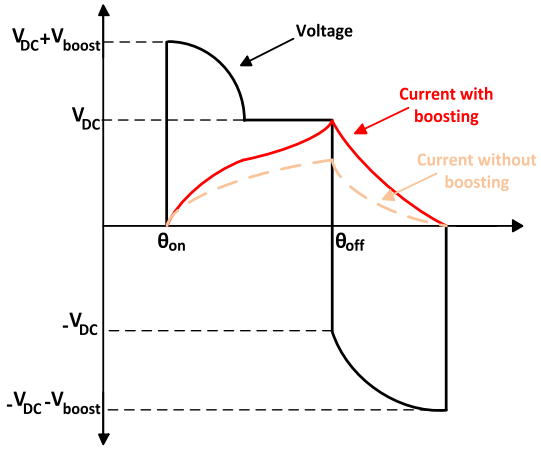

FIGURE 3 Typical voltage and current waveforms in single-pulse mode (no 0 V loops) using voltage-boosting capacitors

induces voltage ($V \propto d\varphi/dt$). The induced voltage produces circulating eddy currents that produce flux ($i \propto \varphi$). The produced flux opposes the original flux from the stator poles. The opposing flux (which increases the effective flux air path length and reduces the effective area) results in decreased effective unaligned inductance. The decrease in the effective unaligned inductance allows a rapid current building up, as demonstrated in Figure 5, which increases the motor output torque.

To gain insight into the effect of rotor conducting screens on the SRM performance, Figure 6 (a) and (b) shows the flux path for unscreened and screened SRMs, respectively, when one stator phase is excited. Figure 6b shows that the reaction field produced by the eddy current in the screen opposes the stator magnetic field, hence preventing the flux lines from crossing through the rotor interpole airgaps as opposed to

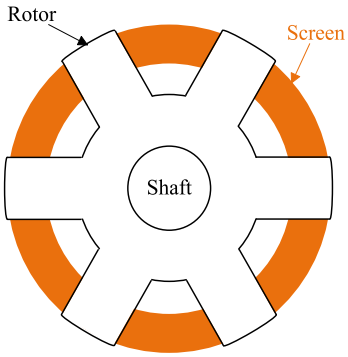

FIGURE 4 Rotor conducting screens in the interpole regions

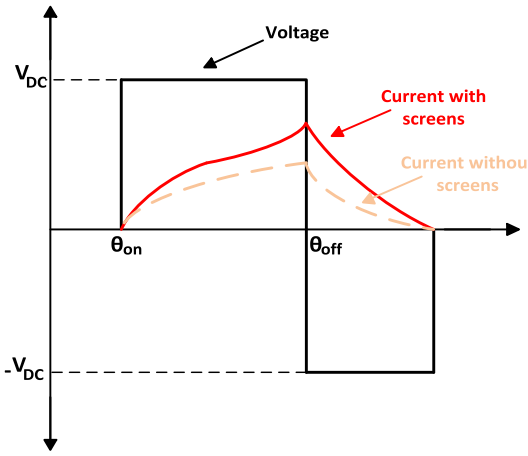

FIGURE 5 SRM voltage and current waveforms with and without conducting screens

Figure 6a. The reluctance path length is increased, and the area is reduced, thus decreasing unaligned inductance.

Figure 7 shows the variation of inductance for half a cycle (from the unaligned to aligned position) for the screened and unscreened SRMs, with the SRM specifications in Table 2. The unscreened SRM has an unaligned inductance of 10.8 mH, while this value is reduced to 4.87 mH in the presence of conducting screens. This 55% decrease in the effective unaligned inductance increases the conversion area (from area OAB to

20429746, 2021, 2, Downloaded from https://ietresearch.onlinelibrary.wiley.com/doi/10.1049/elh2.12012 by NHS Education for Scotland NES, Edinburgh Central Office, Wiley Online Library on [14/11/2022]. See the Terms and Conditions (https://onlinelibrary.wiley.com/terms-and-conditions) on Wiley Online Library for rules of use; OA articles are governed by the applicable Creative Commons License

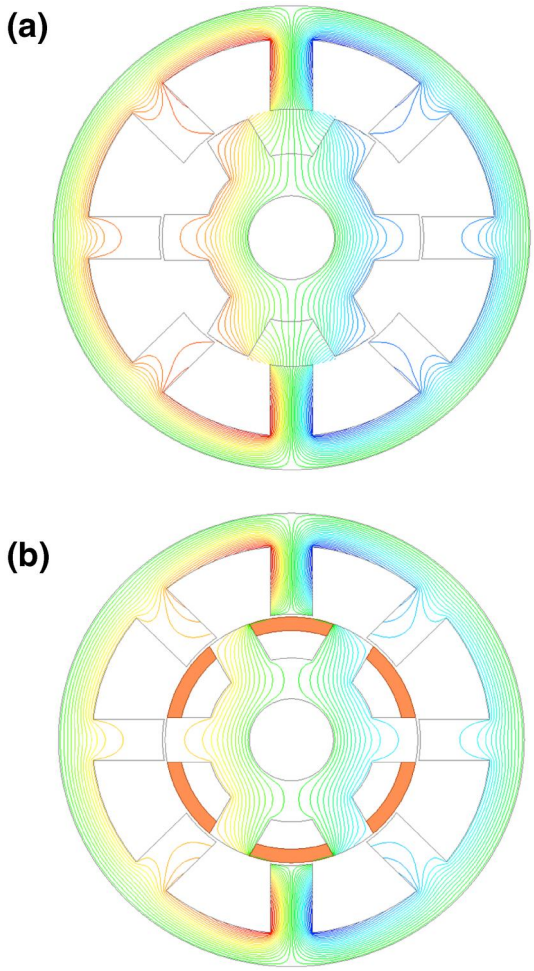

FIGURE 6 Magnetic flux lines: (a) *Unscreened SRM, and* (b) *Screened SRM*

OA'B in Figure 1), thus improving the SRM developed torque. The aligned inductance decreases by 2%, which is insignificant compared with the reduction in the unaligned value.

5 | SCREEN SIMULATION RESULTS

FEA results are presented in this section, where a four-phase, 8/6 SRM with the specification in Table 2 is used for the analysis. The effect of screen material, thickness, and shape on the SRM performance is investigated.

5.1 | Effect of screen material

Figure 8 compares SRM performance at 1500 rpm (base speed) with two different screens. The first screen is 3 mm copper, while the second screen is 15 mm aluminium. The turn on/off angles are the same for the screened and unscreened SRMs, where $\theta_{on} = 32^0$ and $\theta_{off} = 47^0$.

From Figure 8a, the decrease in the effective unaligned inductance accelerates the process of current building-up. As a result, the developed torque increases from 24.1 Nm (unscreened) to 29.25 Nm (screened), as illustrated in Figure 8b. The electrical conductivity of copper is 5.98×10^7 S/m with density 8960 kg/m^3. The electrical conductivity of aluminium is $3.5 \times 10^7 S/m$ with density 2600 kg/m^3.

The SRM with 3 mm copper screens can deliver the same output torque as the 15 mm aluminium screen machine. This highlights that electrical conductivity plays an essential role in the behaviour of the induced eddy current.

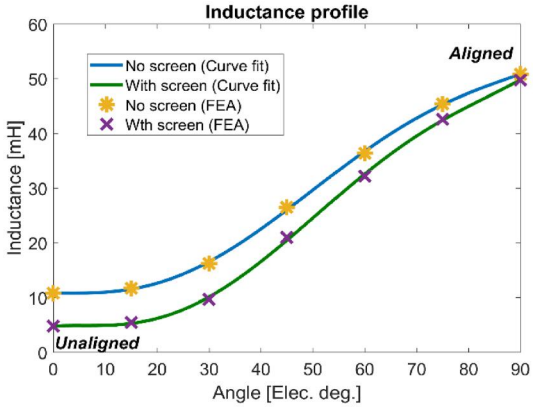

FIGURE 7 Inductance profile

TABLE 2 SRM specifications

Parameter	Value
No. of motor phases m	4
Stator/rotor poles N_s/N_r	8/6
Number of turns per pole N	90
Rated voltage	415 V
Phase winding resistance	0.8 Ω
Rated power	4 kW
Base-speed	1500 rpm
Motor axial length	155 mm
Shaft radius	15 mm
Rotor outer radius	45 mm
Thickness of rotor yoke	15 mm
Ratio of rotor pole arc to pole pitch	0.35
Stator inner radius	46 mm
Stator outer radius	83 mm
Thickness of stator yoke	12 mm
Ratio of stator pole arc to pole pitch	0.42

5.2 | Effect of screen thickness

Figure 9 compares SRM performance when different thickness copper screens are deployed. The turn on/off angles are the same for the screened and unscreened SRM where, $\theta_{on} = 32^0$

20429746, 2021, 2, Downloaded from https://ietresearch.onlinelibrary.wiley.com/doi/10.1049/elp2.12012 by NHS Education for Scotland NES, Edinburgh Central Office, Wiley Online Library on [14/11/2022]. See the Terms and Conditions (https://onlinelibrary.wiley.com/terms-and-conditions) on Wiley Online Library for rules of use; OA articles are governed by the applicable Creative Commons License

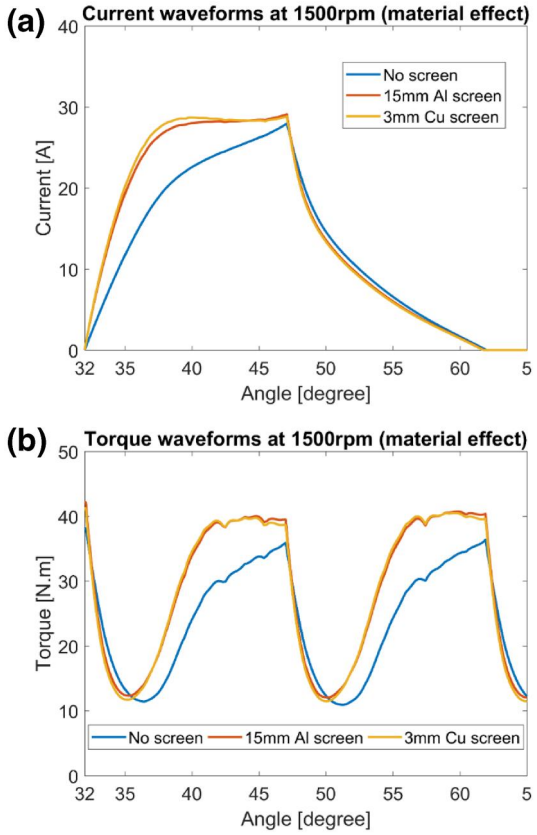

FIGURE 8 Performance of SRM using different screen materials: (a) *Current waveforms, and* (b) *torque waveforms*

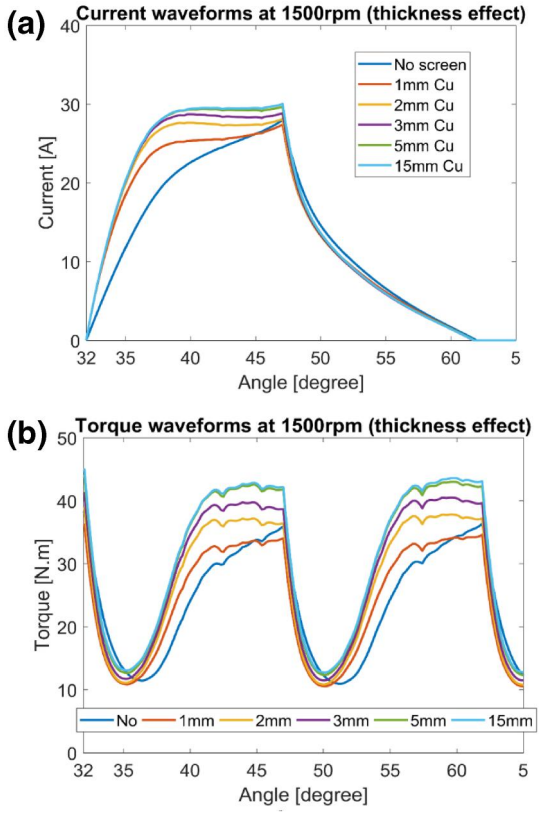

FIGURE 9 Performance of SRM using different screen thickness: (a) *Current waveforms, and* (b) *torque waveforms*

and $\theta_{\text{off}} = 47^0$. The speed is the base speed of 1500rpm. Increasing the screen thickness to fill the entire interpole gap yields the best torque enhancement. However, extra copper (implying more weight and cost) is needed.

This study shows that the screen material's electrical conductivity, along with its thickness, has a significant effect on SRM performance. Using a film screen with low conductivity results in higher resistance to the induced voltage. Hence the eddy current is smaller. Increased resistivity does result in a reduced eddy current decay time constant.

5.3 | Effect of screen shape

The rotor conducting screens relies on the eddy current effect, where eddy current loss in the screens is inevitable. Since machine efficiency is of prime importance in applications as EVs, different screen shapes are compared in terms of developed torque, Cu winding loss, and screen loss. Results for different Cu screen shapes (of around 3–6 mm thick) are summarised in Table 3, where the rotor rotates at 1500 rpm anti-clockwise, with the same turn-on/turn-off angles $\theta_{\text{on}} = 32^0$ and $\theta_{\text{off}} = 47^0$.

The screen shape plays a vital role in determining the developed torque and screen loss, as shown in Table 3. Trimming the conducting screens (as with shape 7 in Table 3) reduces the screen loss. However, a reduction in the developed torque results.

5.4 | Optimal screen selection

From the previous analysis, material, thickness, and shape of the screen have crucially influenced SRM performance. In this sub-section, a multi-objective optimisation problem based on the concept of non-dominated sorting is formulated to elicit the optimum screen with respect to the developed torque, efficiency, and weight of the screen. FEA results for different screens are presented.

5.4.1 | Multi-objective optimisation

In multi-objective optimisation problems, the objective functions are in conflict. Trying to optimise one function may result in a degradation in the other objective functions. Hence, a compromise between these objectives is desirable. Without loss of generality, the optimisation problem is of the form [26]:

$$Minimize\, f(x) = \left[f_1(x),\, f_2(x),\, \ldots,\, f_k(x)\right] \qquad (8)$$

20429746, 2021, 2, Downloaded from https://ietresearch.onlinelibrary.wiley.com/doi/10.1049/elb.2.12012 by NHS Education for Scotland NES, Edinburgh Central Office, Wiley Online Library on [14/11/2022]. See the Terms and Conditions (https://onlinelibrary.wiley.com/terms-and-conditions) on Wiley Online Library for rules of use; OA articles are governed by the applicable Creative Commons License

TABLE 3 Relative FEA performance of different Cu screen shapes at 1500rpm

	Screen	Average o/p torque [N.m]	Winding loss [kW]	Screen loss [kW]
	SRM	24.1	0.44	-
1		30.76	0.625	1.27
2		30	0.6	1.04
3		30.57	0.625	1.29
4		30.26	0.625	1.31
5		30.46	0.63	1.3
6		29.9	0.615	1.34
7		27.34	0.53	0.52

$$subject\ to: \begin{cases} g_{ii}(x) \le 0, & ii = 1,\ 2,\ \ldots,\ y \\ h_{jj}(x) = 0, & jj = 1,\ 2,\ \ldots,\ z \end{cases} \quad (9)$$

where k is the number of objective functions, y is the number of inequality constraints, and z is the number of equality constraints.

There is no single optimal solution in multi-objective optimisation problems, but a set of solutions satisfying a predetermined definition of optimality. Hence, a trade-off between the objectives is achieved according to the perspective of the decision-maker. Converting a multi-objective optimisation problem to a single objective is possible by assigning a suitable weight factor to each objective. However, the optimisation problem will be sensitive to the selected weight factor. Hence, the obtained results may not be satisfactory [27].

A Pareto optimal (non-dominated) solution is a point that improves at least one objective without retrograding the remaining objectives [28]. The set of Pareto optimal solutions is called a Pareto frontier. Usually, it is preferable to know all the Pareto frontier solutions to allow the designer to select the most adequate solution among different alternatives. The problem of generating the Pareto frontier is based on non-dominated sorting, where all the solutions are compared with select the non-dominated ones. Hence, non-dominated sorting is applied to assess the obtained solutions [29, 30].

5.4.2 | FEA screen results

Since the theory of rotor conducting screens relies on the eddy current effect, screen eddy current loss is inevitable. As machine efficiency is of prime importance, different screen shapes are compared in terms of developed torque, the weight of added material, and efficiency to elicit the best screen candidates (generating the Pareto frontier). Thus, an optimisation problem is formulated based on (8) and (9) with maximising the developed torque and efficiency while minimising the weight of added material. At least a 10% improvement in developed torque is set as a constraint.

More than 100 screens shapes are compared, with rotor rotating at 1500 rpm anti-clockwise rotation, using the same turn-on/turn-off angles with $\theta_{on} = 32^0$ and $\theta_{off} = 47^0$. Shapes of screens representing the Pareto frontier are shown in Figure 10, with the results summarised in Table 4.

The results presented in Table 4 represent the optimum screen designs. Each screen is a trade-off between the three objective functions viz., developed torque, the weight of added material, and efficiency.

A 3.5 cost ratio between copper and aluminium suggests that aluminium screens are lighter and cheaper than copper screens. However, torque improvement using aluminium screens is inferior to that of copper screens.

Shifting the screen below the rotor pole tip (as in designs 'b', 'c', and 'd') slightly increases the flux path area, hence minorly increasing the unaligned inductance compared with design 'a'. This slight increase in the inductance reduces the phase current, hence the eddy current loss, improving the efficiency. However, this improvement in efficiency (compared with design 'a') is at the cost of reducing the developed torque (i.e. design 'a' produces the highest torque with the lowest efficiency). Designs 'b', 'c', and 'd' improve the efficiency of design 'a' with a slight reduction in torque.

Results summarised in Table 4 represent the Pareto optimal results for the investigated 8/6 SRM. Any screen represents an optimal solution with a trade-off between developed torque, efficiency, and added material weight. These three aspects are of prime importance in EV applications. The efficiency directly relates to the vehicle range. Hence, increasing efficiency allows increasing the covered range with the same battery size.

20429746, 2021, 2, Downloaded from https://ietresearch.onlinelibrary.wiley.com/doi/10.1049/elh2.12012 by NHS Education for Scotland NES, Edinburgh Central Office, Wiley Online Library on [14/11/2022]. See the Terms and Conditions (https://onlinelibrary.wiley.com/terms-and-conditions) on Wiley Online Library for rules of use; OA articles are governed by the applicable Creative Commons License

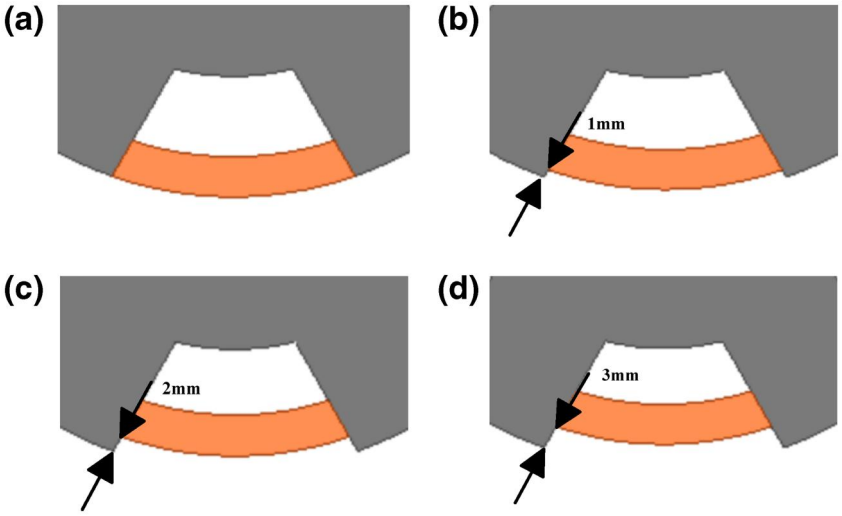

FIGURE 10 Optimum screen designs: (a) *design a,* (b) *design b,* (c) *design* (c), *and* (d) *design* (d)

TABLE 4 Screens Pareto optimal frontier

Screen	Material	Thickness [mm]	Screen weight [kg/m]	Increase in o/p torque [%]	Efficiency [%]
SRM	-	-	-	-	89.56
Sc-a	Al	3	1.36	11.75	69.0
		4	1.78	15.90	70.0
		5	2.18	18.47	70.9
		6	2.57	20.00	71.5
		7	2.94	20.80	71.9
	Cu	4	6.13	26.00	71.0
		5	7.53	28.20	71.9
		6	8.86	29.30	72.4
Sc-b	Al	4	1.70	12.60	73.8
		5	2.10	14.57	74.5
		6	2.47	15.57	75.0
	Cu	4	5.90	20.60	74.6
		5	7.24	21.50	76.5
Sc-c	Al	5	2.00	11.30	77.4
		6	2.37	12.10	77.8
	Cu	4	5.68	15.94	77.5
		5	6.96	17.35	78.2
Sc-d	Cu	4	5.46	12.70	80.0
		5	6.68	13.50	80.4

On the other hand, the output torque, along with the motor weight, determines the machine's torque and power density, reflecting on the base speed and motor acceleration. The decision-maker can choose any screen from Table 4 depending on any constraints dictated by his/her application. For example, if more than 75% efficiency and an increase in output torque of more than 20% are required. Hence, a 5 mm Cu screen of design 'b' is selected.

20429746, 2021, 2, Downloaded from https://ietresearch.onlinelibrary.wiley.com/doi/10.1049/elh2.12012 by NHS Education for Scotland NES, Edinburgh Central Office, Wiley Online Library on [14/11/2022]. See the Terms and Conditions (https://onlinelibrary.wiley.com/terms-and-conditions) on Wiley Online Library for rules of use; OA articles are governed by the applicable Creative Commons License

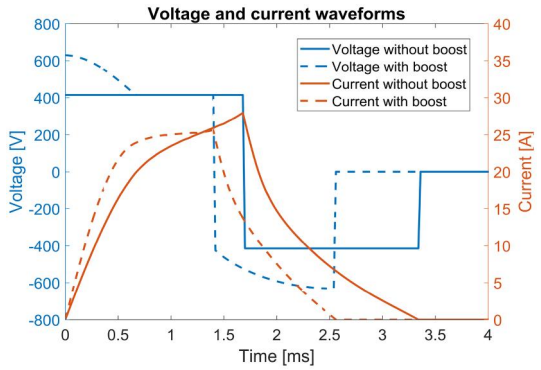

FIGURE 11 Voltage and current waveforms with and without voltage boosting

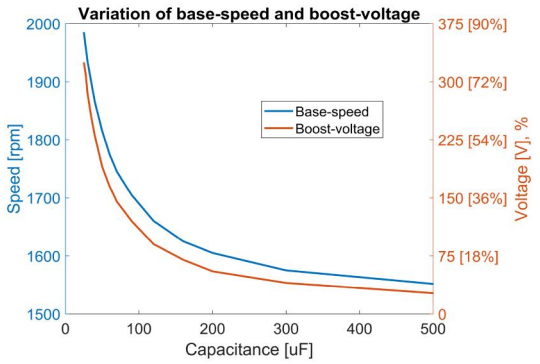

FIGURE 12 Variation of base speed and boost voltage with capacitance

6 | SRM PERFORMANCE WITH DC-LINK VOLTAGE BOOSTING

In this section, SRM performance with voltage boosting is demonstrated. The 4φ, 8/6 SRM with the specification in Table 2, is used.

The energy associated with the outgoing phase windings is fed-back to the boost-capacitors (due to the blocking diodes D_{x2} and D_{y2}). The increased capacitor voltages (well above the DC-link voltage) accelerates the current build-up in the incoming phase windings. This is established in Figure 11, which shows the voltage and current waveforms with and without boost-capacitors.

Capacitors of 47.5 μF, >600 V are used. The same turn on and turn off angles are used in both cases, with $\theta_{on} = 32^0$ and $\theta_{off} = 47^0$. The SRM base speed without voltage boosting is 1500 rpm. This value rises to 1810 rpm with voltage boosting, as indicated in Figure 11 (same dwell period with higher speed implies a shorter time).

The increased voltage at turn on and turn off (above the source voltage of 415 V DC) increases the phase current rate of change hence increasing the base speed (at full load torque). The variation of base speed and boost voltage with capacitance is given in Figure 12.

The increasing base speed and boost voltage with decreasing capacitance are commensurate with increased semiconductor voltage stresses. Table 5 illustrates the cost comparison between converters without and with voltage boosting, excluding the regenerative braking circuit cost.

The converter is tested experimentally. The specifications of the 8/6 SRM, used for experimentation, are given in Table 2, while Figure 13 shows the test rig. A DC source voltage of 100 V is utilised, the boosting capacitors are 40 μF (±10%), and the sampling frequency is 20 kHz. Figure 14 shows the SRM performance without and with voltage boosting, respectively. The extra voltage offered by the boost capacitors allows the current of the incoming phase to build up quickly, thus quickly increasing the motor speed from 380 to 660 rpm at the same load torque. Also, the outgoing phase current decays faster in the presence of the increasing boost voltage. The exaggerated improvement in the motor speed obtained experimentally (around 75%) is due to the accentuated boost voltage compared with DC source voltage.

7 | POWER DENSITY IMPROVEMENT WITH ROTOR CONDUCTING SCREENS AND DC-LINK VOLTAGE BOOSTING

In this section, the performance of SRM with rotor conducting screens and DC-link voltage boosting is investigated. The power density of the designed SRM with rotor conducting screens and voltage boosting is compared with the power density of an equivalent-sized PMSM. The PMSM used for comparison is the traction motor deployed in third-generation Toyota Prius, 2010 [31].

The main PMSM specifications are given in Table 6, used as constraints for designing the proposed SRM.

A 4φ 16/12 SRM is selected. A higher number of poles reduces the torque ripple, which is required in EV applications. The stator outer diameter and the motor axial length are 264 and 108 mm, respectively, similar to the benchmarked PMSM. Usually, the stator outer diameter is 1.5 times the rotor outer diameter [32]. Hence, the rotor outer diameter is selected to be 176 mm. A typical air-gap length for SRM is between 0.25 and 1 mm. It is worth to highlight that small air gaps are not adequate in EV applications. The drivetrain is affected by road conditions that may produce severe vibration and mechanical stress [33]. Therefore, a 0.5 mm air gap is selected.

Selecting adequate stator and rotor pole arcs is of prime importance. Miscalculations could lead to self-starting problems. Hence, to assure torque production at all rotor positions, the stator pole arc is calculated using (10)

$$\beta_s \geq \frac{2\pi}{mN_r} \tag{10}$$

Usually, the stator pole arc is selected slightly smaller than the rotor pole arc to allow more stator slot area to accommodate the winding. For achieving a complete unaligned position, Equation (11) should be satisfied.

20429746, 2021, 2, Downloaded from https://ietresearch.onlinelibrary.wiley.com/doi/10.1049/els2.12012 by NHS Education for Scotland NES, Edinburgh Central Office, Wiley Online Library on [14/11/2022]. See the Terms and Conditions (https://onlinelibrary.wiley.com/terms-and-conditions) on Wiley Online Library for rules of use; OA articles are governed by the applicable Creative Commons License

TABLE 5 Cost comparison between converters without and with voltage boosting

	Point	Converter without boost	Converter with boost
Main switches	No. of switches	6	6
	Part number	IXFR48N60P	IXFK32N80P
	Voltage rating	600 V	800 V
	Current rating	32 A	32 A
	Cost/switch	£ 8.81	£ 7.49
	Total switches cost	***£52.86***	***£44.94***
Main diodes	No. of diodes	6	6
	Part number	STTH30L06GYTR	DSI30-08A
	Voltage rating	600 V	800 V
	Current rating	30 A	30 A
	Cost/diode	£1.82	£1.56
	Total diodes cost	***£10.92***	***£9.36***
Boost capacitors	No. of capacitors	-	2
	Part number	-	B32778Z8506K000
	Voltage rating	-	800V
	Capacitance	-	50 μF (±10%)
	Cost/capacitor	-	£7.68
	Total capacitors cost	**-**	***£15.36***
Blocking diodes	No. of diodes	-	2
	Part number	-	STTH30R04G
	Voltage rating	-	400V
	Current rating	-	30A
	Cost/diode	-	£2.05
	Total diodes cost	**-**	***£4.1***
	Total converter cost	***£63.78***	***£73.76***

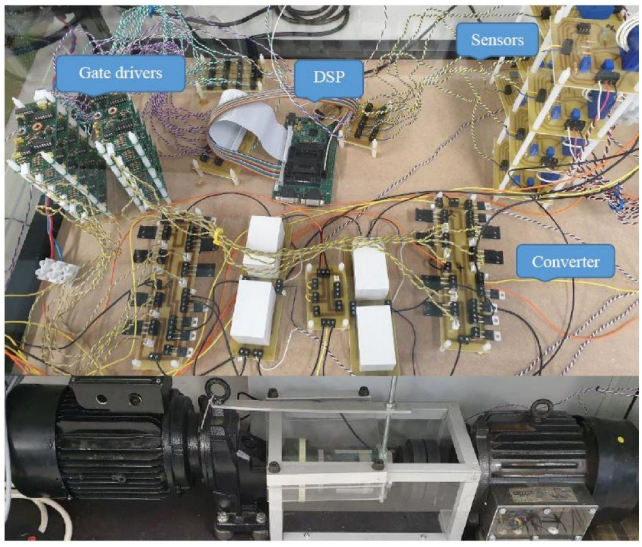

FIGURE 13 Experimental test rig

$$\beta_s + \beta_r < \frac{2\pi}{N_r} \tag{11}$$

The selected stator and rotor pole arcs are 10^0 and 12^0, respectively.

Large stator back iron is desirable to reduce vibration, increase mechanical strength, and ease saturation. However, an excessively large value will reduce the available space for stator winding. The rotor back iron has the same constraint as the stator back iron regarding saturation. The rotor pole height should be several times larger than the air gap to increase the conversion area (reducing the unaligned inductance). Hence, (12) gives an initial value for the stator and rotor pole heights and back iron, respectively.

$$h_s,\ h_r,\ b_{sy}, b_{ry} > \frac{d}{2} \sin \beta_r/2 \tag{12}$$

where d is the rotor outer radius.

20429746, 2021, 2, Downloaded from https://ietresearch.onlinelibrary.wiley.com/doi/10.1049/elh2.12012 by NHS Education for Scotland NES, Edinburgh Central Office, Wiley Online Library on [14/11/2022]. See the Terms and Conditions (https://onlinelibrary.wiley.com/terms-and-conditions) on Wiley Online Library for rules of use; OA articles are governed by the applicable Creative Commons License

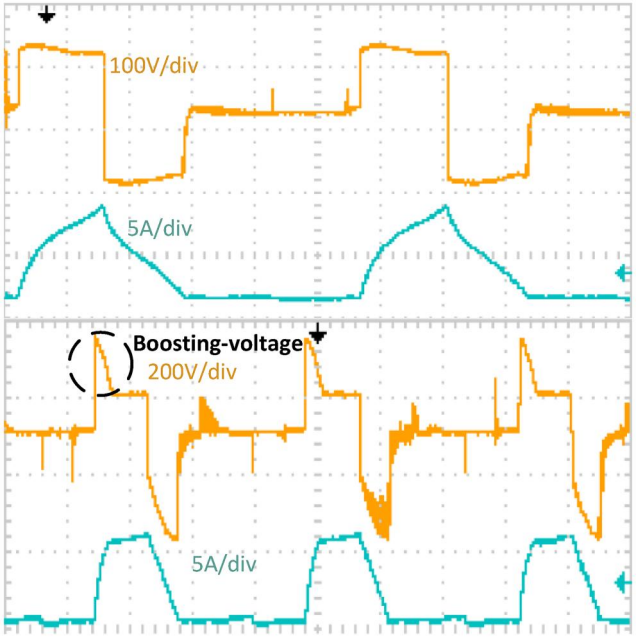

FIGURE 14 Experimental voltage and current waveforms without and with voltage boosting

TABLE 6 PMSM specifications

Parameter	Value
Stator outer diameter	264 mm
Motor axial length	108 mm
DC-link voltage	650 V
Peak current	240 A
RMS current	141 A
Slot fill factor	0.54
Current density	19 A/mm^2
Rated power	60 kW
Rated torque	207 N.m
Base-speed	2760 rpm

The stator and rotor pole heights and back iron are 23.5 and 15, 20, and 48 mm, respectively.

Finally, the motor axial length is the sum of the stack length and coil end length [34]. Hence, the stack length defined by (13) is calculated to be 86 mm.

$$L_s = L_{axial} - \frac{\pi}{N_s}\left(D/2 - b_{sy}\right) \tag{13}$$

where L_s is the stack length, L_{axial} is the motor axial length, and D is the stator outer diameter.

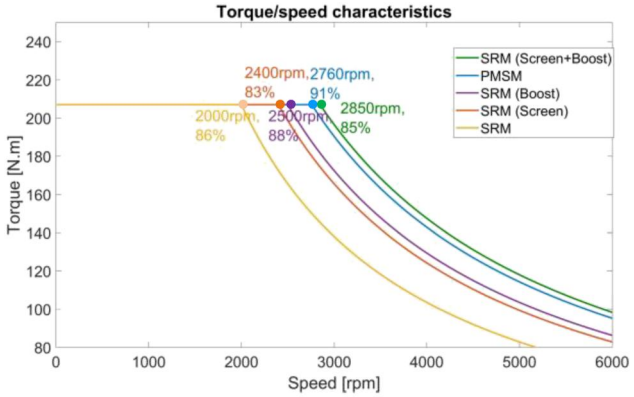

FIGURE 15 Torque/speed characteristics

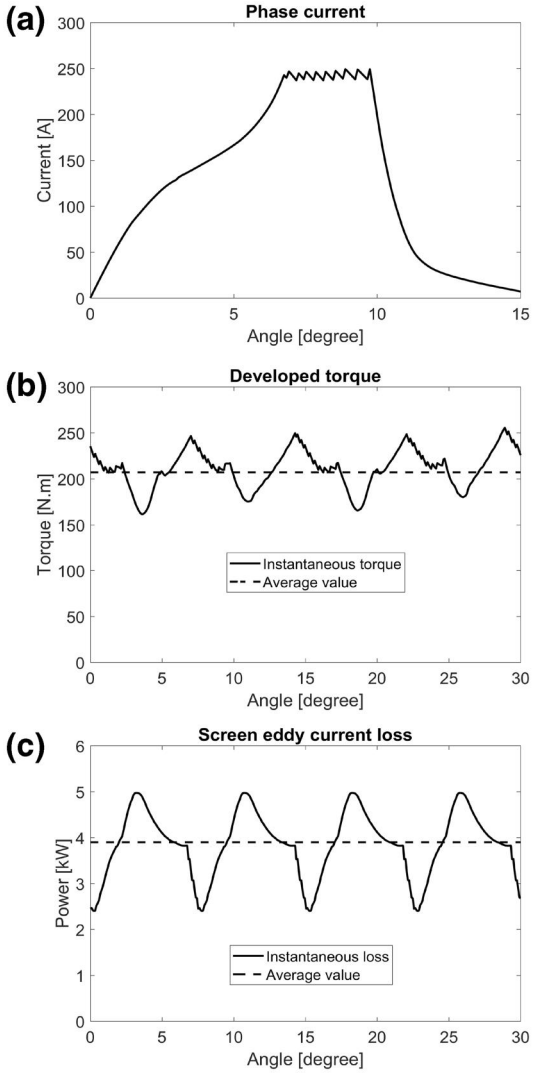

FIGURE 16 Performance of SRM with screens and voltage boosting: (a) *phase current,* (b) *developed torque, and* (c) *screen eddy current loss*

Figure 15 shows the torque/speed curve with efficiency for five different motors, namely; PMSM, designed SRM, SRM with rotor conducting screens, SRM with voltage boosting, and

20429746, 2021, 2, Downloaded from https://ietresearch.onlinelibrary.wiley.com/doi/10.1049/elh2.12012 by NHS Education for Scotland NES, Edinburgh Central Office, Wiley Online Library on [14/11/2022]. See the Terms and Conditions (https://onlinelibrary.wiley.com/terms-and-conditions) on Wiley Online Library for rules of use; OA articles are governed by the applicable Creative Commons License

TABLE 7 Comparison between PMSM and SRM with rotor conducting screens and DC-link voltage boosting

Parameter	PMSM	SRM with screens and boost
Stator outer diameter	264 mm	264 mm
Motor axial length	108 mm	108 mm
DC-link voltage	650 V	650 V (+50% boost)
Peak current	240 A	240 A
rms current	141 A	107 A
Slot fill factor	0.54	0.54
Current density	19 A/mm^2	16.7 A/mm^2
Rated power	60 kW	62 kW
Rated torque	207 N.m	207 N.m
Base-speed	2760 rpm	2850 rpm
Efficiency at knee-point	91%	85%

finally SRM with both rotor conducting screens and DC-link voltage boosting.

The PMSM has a base-speed of 2760 rpm at 207 N.m output torque. The base-speed of the designed SRM at 207 N.m is 2000 rpm. SRM with rotor conducting screens (4 mm aluminium screen, 6 mm below pole tip as per Figure 10) and SRM with DC rail voltage boost (50% voltage boosting, 52.5 μF) increase the speed at which full-load torque can be delivered from 2000 to 2400 rpm and 2500 rpm, respectively, hence improving the power-to-weight ratio by 20% and 25%, respectively. SRM with rotor conducting screens and DC-link voltage boosting improves the base-speed to 2850 rpm, which is competitive with PMSM.

Figure 16 shows the performance of SRM with DC-link voltage boosting and rotor conducting screens. The peak current is limited to 240 A, as illustrated in Figure 16a with 107A rms value. Figure 16b shows the instantaneous developed torque with a 207 N.m average value. Finally, Figure 16c shows the inevitable screen eddy current loss having an average value of 3.9 kW.

Table 7 compares the PMSM with SRM with rotor conducting screens and DC-link voltage boosting, revealing that SRM can compete in the EV market.

8 | CONCLUSION

The effect of utilising rotor conducting screens along with DC-link voltage boosting-capacitors to enhance SRM performance is studied. The effect of using conducting screens of different materials, thicknesses, and shapes on SRM performance was presented. Using a film screen with low conductivity results in higher resistance to the induced voltage. Hence, the eddy current is smaller. Increased resistivity results in a reduced eddy current decay time constant.

A multi-objective optimisation problem based on non-dominated sorting was formulated to elicit the optimum screen shape. Four designs are advised with respect to the developed torque, efficiency, and weight of added material. A 3.5 cost ratio between copper and aluminium suggests that aluminium screens are lighter and cheaper than copper screens. However, torque improvement using aluminium screens is inferior to that of copper screens. Shifting the screen below the rotor pole tip (below the air gap) offers a trade-off between developed torque and efficiency.

DC-link voltage boosting improves the power-to-weight performance but with increased semiconductor voltage stresses as a consequence of boost capacitor voltages during excess DC voltage source. An SRM with rotor conducting screens and DC-link voltage boosting improves SRM power-to-weight ratio to be competitive with an equivalent PMSM, but with the penalty of inevitable screen eddy current loss.

ACKNOWLEDGEMENT

The publication of this article was funded by NPRP grant NPRP (9-092-2-045) from the Qatar National Research Fund (a member of Qatar Foundation).

ORCID

Aly A. Abdel-Aziz https://orcid.org/0000-0003-1681-7966

REFERENCES

1. Habib, S., et al.: A comprehensive study of implemented international standards, technical challenges, impacts and prospects for electric vehicles. IEEE Access. 6, 13866–13890 (2018)
2. Yang, Z., et al.: Comparative study of interior permanent magnet, induction and switched reluctance motor drives for EV and HEV applications. IEEE Trans. Transp. Electr. 1(3), 245–254 (2015)
3. Zaraoulia, M., Benbouzid, M., Diallo, D.: Electric motor drive selection issues for HEV propulsion systems: a comparative study. IEEE Trans. Veh. Technol. 55(6), 1756–1764 (2006)
4. Bostanci, E., et al.: Opportunities and challenges of switched reluctance motor drives for electric propulsion: a comparative study. IEEE Trans. Transp. Electr. 3(1), 58–75 (2017)
5. Rahman, K., et al.: Advantages of switched reluctance motor applications to EV and HEV: design and control issues. IEEE Trans. Ind. Appl. 36(1), 111–121 (2000)
6. Wang, S., et al.: Implementation of a 50-KW four-phase switched reluctance motor drive system for hybrid electric vehicle. IEEE Trans. Magn. 41(1), 501–504 (2005)
7. Chiba, A., et al.: Torque density and efficiency improvements of a switched reluctance motor without rare-earth material for hybrid vehicle. IEEE Trans. Ind. Appl. 47(3), 1240–1246 (2011)
8. Takeno, M., et al.: Test results and torque improvement of the 50-KW switched reluctance motor designed for hybrid electric vehicles. IEEE Trans. Ind. Appl. 48(4), 1327–1334 (2012)
9. Chiba, A., et al.: Development of rare-earth-free SR motor with high torque density for hybrid vehicles. IEEE Trans. Energy Conv. 30(1), 175–182 (2015)
10. Jiang, J., Bilgin, B., Emadi, A.: Three-phase 24/16 switched reluctance machine for a hybrid electric powertrain. IEEE Trans. Transp. Electr. 3(1), 76–85 (2017)
11. Kiyota, K., Chiba, A.: Design of switched reluctance motor competitive to 60-kW IPMSM in third-generation hybrid electric vehicle. IEEE Trans. Ind. Appl. 48(6), 2303–2309 (2012)
12. Kiyota, K., et al.: Comparison of the test result and 3D-FEM analysis at the knee point of a 60 kW SRM for a HEV. IEEE Trans. Magn. 49(5), 2291–229 (2013)

20429746, 2021, 2, Downloaded from https://ietresearch.onlinelibrary.wiley.com/doi/10.1049/elp2.12012 by NHS Education for Scotland NES, Edinburgh Central Office, Wiley Online Library on [14/11/2022]. See the Terms and Conditions (https://onlinelibrary.wiley.com/terms-and-conditions) on Wiley Online Library for rules of use; OA articles are governed by the applicable Creative Commons License

13. Kiyota, K., Kakishima, T., Chiba, A.: Comparison of test results and design stage prediction of switched reluctance motor competitive with 60-kW rare-earth PM motor. IEEE Trans. Ind. Electron. 61(10), 5712–5721 (2014)
14. Hutton, A., Miller, T.: Use of flux screens in switched reluctance motors. In: IEEE 4th international conf. on Electrical Machines and Drives, London, pp. 312–316.September, 1989
15. Dessouky, Y., Williams, B., Fletcher, J.: Conducting screen utilization in switched reluctance motors. IEEE Trans. Energy Convers. 14(4), 946–951 (1999)
16. Hamdy, R., et al.: High-speed performance improvements of a two-phase switched reluctance machine utilizing rotor-conducting screens. IEEE Trans. Energy Convers. 17(4), 500–506 (2002)
17. Mahmoud, M., Fletcher, J., Williams, B.: Evaluation of rotor conducting screens on the rotor of the single-phase switched reluctance machine. In: IEEE 2nd international conf. on Power Electron., Machines and Drives, pp. 18–23.March, Edinburgh (2004)
18. Chan, S., Bolton, H., Performance enhancement of single-phase switched-reluctance motor by DC link voltage boosting. Proc. Inst. Elect. Eng. 140(5), 316–322 (1993)
19. Barnes, M., Pollock, C.: Power converter for single phase switched reluctance motors. Electron. Lett. 31(25), 2137–2138 (1995)
20. Dahmane, M., Meibody, F., Sargos, F.: An adaptive converter for switched reluctance motor/generator for high speed applications. In: Proc. Ind. Appl. Conf. pp. 1547–1554.Rome, Italy (October, 2000)
21. Lee, D., Ahn, J.: A novel four-level converter and instantaneous switching angle detector for high speed SRM drive. IEEE Trans. Power Electron. 22(5), 2034–2041 (2007)
22. Liang, J., et al.: Analysis of passive boost power converter for three-phase SR drive. IEEE Trans. Ind. Electron. 57(9), 2961–2971 (2010)
23. Dessouky, Y., Williams, B., Fletcher, J.: A novel power converter with voltage-boosting capacitors for a four-phase switched reluctance motor drive. IEEE Trans. Ind. Electron. 45(5), 815–823 (1998)
24. Abdel-Aziz, A., et al.: A neutral-point diode-clamped converter with inherent voltage-boosting for a four-phase SRM drive. IEEE Trans. Ind. Electr. 67(7), 5313–5324 (2020)
25. Krishnan, R.: Switched reluctance motor drives: modelling, simulation, analysis, design and applications. CRC Press, Boca Raton, FL (2001)
26. Fei, Z., et al.: A survey of multi-objective optimization in wireless sensor networks: metrics, algorithms and open problems. IEEE Comm. Surv. Tut. 19(1), 550–586 (2017)
27. Fang, H., et al.: An efficient non-dominated sorting method for evolutionary algorithms. Evol. Comput. 16(3), 355–384 (2008)
28. Zhang, X., et al.: An efficient approach to non-dominated sorting for evolutionary multi-objective optimization. IEEE Trans. Evol. Comput. 19(2), 210–213 (2015)
29. Deb, K., et al.: A fast and elitist multi-objective genetic algorithm: NSGA-II. IEEE Trans. Evol. Comput. 6(2), 182–197 (2002)
30. Clymont, KM., Keedwell, E.: Deductive sort and climbing sort: new methods for non-dominated sorting. Evol. Comput. 20(1), 1–26 (2012)
31. Burress, T., et al.: Evaluation of the 2010 Toyota Prius hybrid synergy drive system (Report No. ORNL/TM-2010/253). Oak Ridge National Laboratory. Oak Ridge, TN (2011)
32. Chau, K.: Switched reluctance motor drives. In: Electric vehicle machines and drives: design, analysis and application, pp. 108–146.IEEE (2015)
33. Bilgin, B., Emadi, A., Krishnamurthy, M.: Design considerations for switched reluctance machines with a higher number of rotor poles. IEEE Trans. Ind. Electron. 59(10), 3745–3756 (2012)
34. Kiyota, K., Nakano, S., Chiba, A.: A fast calculation method of optimal ratio of outer diameter and axial length for torque improvement in switched reluctance motor. IEEE Trans. Ind. Appl. 54(6), 5802–5811 (2018)

How to cite this article: Abdel-Aziz AA, Ahmed KH, Massoud AM, Williams BW. SRM power density improvement utilising rotor conducting screens and DC-link voltage boosting for EV applications. *IET Electrical Systems Transp*. 2021;11:148–160. https://doi.org/10.1049/els2.12012

20429746, 2021, 2, Downloaded from https://ietresearch.onlinelibrary.wiley.com/doi/10.1049/els2.12012 by NHS Education for Scotland NES, Edinburgh Central Office, Wiley Online Library on [14/11/2022]. See the Terms and Conditions (https://onlinelibrary.wiley.com/terms-and-conditions) on Wiley Online Library for rules of use; OA articles are governed by the applicable Creative Commons License